Synthetic Metals 226 (2017) 7–14

Contents lists available at ScienceDirect

Synthetic Metals

journal homepage: www.elsevier.com/locate/synmet

Electrically conductive nanocomposites for fused deposition modelling

A. Dorigato[a,*], V. Moretti[a], S. Dul[a], S.H. Unterberger[b,c], A. Pegoretti[a]

[a] University of Trento, Department of Industrial Engineering and INSTM Research Unit, Via Sommarive 9, 38123 Trento, Italy
[b] Unit for Material Technology, University of Innsbruck, Austria
[c] Christian Doppler Laboratory for Cement and Concrete Technology, Technikerstraße 13, 6020 Innsbruck, Austria

ARTICLE INFO

Article history:
Received 23 September 2016
Received in revised form 9 January 2017
Accepted 12 January 2017
Available online xxx

Keywords:
Acrylonitrile-butadine-styrene
Carbon nanotubes
Fused deposition modelling
Nanocomposites
Electrical resistivity

ABSTRACT

An acrylonitrile-butadiene-styrene (ABS) matrix was melt compounded with various amounts (from 1 to 8 wt%) of multi-walled carbon nanotubes (MWCNT) predispersed in an ABS carrier. The resulting materials were then i) compression molded (CM) to obtain plaques or ii) extruded in filaments used to feed a fused deposition modelling (FDM) machine. 3D printed samples were obtained under three different orientations.

The nanofiller addition within the ABS matrix caused a remarkable increase of both stiffness and stress at yield of the bulk samples, accompanied by a strong reduction of the elongation at break. The mechanical properties of 3D printed samples resulted to be strongly dependent on the printing orientation. The addition of CNTs was very effective in improving the electrical conductivity with respect to neat ABS even at the smallest filler content. The FDM process determined a partial loss in the electrical conductivity of ABS nanocomposites, with a marked dependency on the printing orientation. For CNT amounts higher than 4 wt%, CM samples manifested a rapid heating by Joule effect, while the process was less efficient in the printed samples. CNT addition has high impact on thermal properties, resulting in a decrease of specific heat and a increase of thermal diffusivity and conductivity. Like observed for electric conductivity FDM also influences properties of thermal diffusivity and conductivity, resulted by a possible orientation of CNT.

1. Introduction

In the last years, polymer matrix nanocomposites have attracted a remarkable interest because nanoscale affects the potential to lead significant improvements in properties such as impact resistance [1], elastic modulus [6], thermal stability and fire resistance [2–5] compared with those of neat polymers. It is well known that conventional polymers offer significant resistance to electrical conduction [7] and several methods have been explored to increase their electrical conductivity values [8,9]. One of the most promising methods is to add conductive fillers such as carbon black, CNTs or metal particles to polymer matrices. In fact, above a critical concentration (i.e. percolation threshold), it is possible to observe the formation of a conductive path within the polymer matrix constituted by uninterrupted clusters of connected filler particles [10–12]. These materials can be used in applications where charge dissipation and electrical conductivity are desired, such as films for packaging of sensitive electronics components or materials subjected to corona treatments. Considering that an inhomogeneous dispersion in filled polymers can lead to problems such as heavy process dependency, the control of the filler dispersion quality represents one of the most critical and challenging technical issue.

Fused deposition modelling (FDM) is an emerging technology, and represents one of the most common techniques for prototyping and personal additive manufacturing [13]. This is an extrusion based system, in which a thermoplastic polymer is supplied as a continuous solid filament. It is pushed into a heating chamber by a tractor wheel arrangement and it is heated until softening or melting. The extrusion pressure is given by the portion of filament pushed into the chamber that forces the softened material through the nozzle. The extruder head is able to scan on a horizontal plane as well as starting and stopping the flow of material; in addition the deposition bed can move in the vertical direction. In fact, once a layer is completed, the bed moves the part downwards, so that a further layer can be produced. In order to obtain a flow of material with constant rate and constant cross-section diameter, the extrusion pressure and the travel speed of the nozzle across a depositing surface must remain as constant as possible during all deposition phases. The technical improvements

* Corresponding author.
E-mail address: andrea.dorigato@ing.unitn.it (A. Dorigato).

http://dx.doi.org/10.1016/j.synthmet.2017.01.009
0379-6779/

obtained for this technology over the last 25 years attracted a strong interest from both academy and industry [14]. The relative easiness of use and the affordable cost for entry-level machines gave this technology the ability of changing the common conception of how things can be produced, opening new possibility of manufacturing complex products with limited economical investments. As other additive manufacturing processes, this technology allows to produce small complex parts at low volumes, reducing the need of moulds or tools. Therefore, it can compete on cost and delivery speed with traditional manufacturing processes for products that need short production runs. Various polymeric materials have been explored for application in FDM, however commercial FDM machines mostly use acrylonitrile butadiene styrene (ABS) and polylactic acid (PLA).

In literature is well reported how the electrical conductivity of ABS could be strongly increased by nanofiller addition. As an example, in a paper of Saleh et al. [15], a nanocomposite with carbon nanotube (CNT) dispersed in a ABS matrix was prepared by solution mixing. The good dispersion and selective localization of CNT in the styrene acrylonitrile styrene (SAN) phase of the ABS matrix allowed to prepare nanocomposites with a percolation threshold of only 0.06 vol%. Moreover, the addition of nanofillers to ABS has recently emerged as a possible tool to increase the mechanical properties of filaments for FDM applications [16–19].

On the basis of these considerations, the objective of the present work is to investigate the mechanical, electrical and thermal behaviour of ABS/CNT nanocomposites for FDM applications. A comparison between the properties of the bulk (compression molded) and 3D printed samples (along different orientations) was carried out, in order to underline the role of the filler content and of the manufacturing procedure on the physical properties of the prepared materials. Furthermore, the possibility to heat 3D printed parts by Joule effect has been experimentally proven.

2. Experimental part

2.1. Materials

A Sinkral PD L 322 ABS, produced by Versalis-Eni (Mantova, Italy) using a continuous mass polymerization process, was utilized as polymeric matrix (density 1.04 g/cm^3, MFI at 220 °C 10 kg 23 g/10 min). An ABS/CNT masterbatch, Plasticyl ABS1501 produced by Nanocyl S.A. (Sambreville, Belgium), was utilized. According to the manufacturer this masterbatch contains 15 wt% of NC7000 multi-walled carbon nanotubes (MWCNTs) produced by Nanocyl S.A. (Sambreville, Belgium).

2.2. Samples preparation

In this work, two different manufacturing processes were used for the production of the samples. The bulk materials were produced through a melt compounding process followed by compression molding, while 3D printed materials were prepared by using a FDM machine starting from extruded filaments. ABS pellets and masterbatch were preliminary dried at a temperature of 80 °C for 4 h with an air flow of 7 m^3/h by using a Moretto X Dry air drier. Nanocomposite samples were then melt compounded in a Thermo Haake Polylab internal mixer at 190 °C for 15 min, setting a rotor speed of 90 rpm. A compression molding process was then performed at 200 °C with a pressure of 3.8 MPa for 10 min, in order

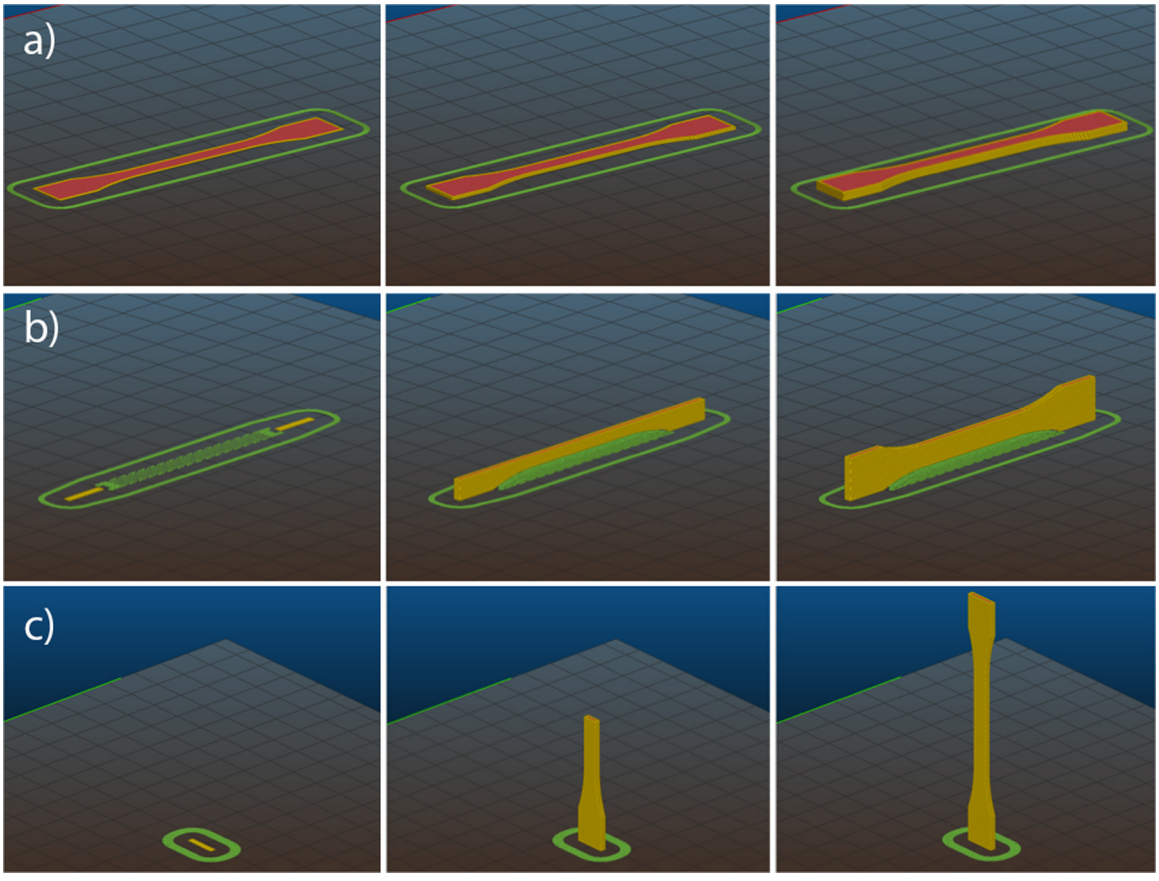

Fig. 1. Rendering of the 3D printing of samples in different directions: a) horizontal (HC), b) vertical (VC), c) perpendicular (PC) building orientations.

to produce square sheeets of composite samples with an average thickness of 1.0 mm.

A part of the bulk samples was mechanically grinded, and the resulting pellets were used to feed a Thermo-Haake Rheomex co-rotating intermeshing twin-screw extruder characterized by a screw diameter of 16 mm and L/d ratio of 25. The processing temperatures along the barrel were set at 180, 210, 220, 230 and 240 °C starting from the feeding hopper to the extrusion die. Due to the higher melt viscosity induced by CNT, a screw speed of 5 rpm was used for the filled materials while it was increased up to 10 rpm for neat ABS. The extruder was equipped with a circular die with a diameter of 1.65 mm that allowed the production of filaments with a diameter of 1.44 ± 0.02 mm suitable for the FDM process.

3D models were realized by AutoCAD 2016 and they were then exported in STL format. Silc3r was employed for the slicing of STL file and for setting up the printing parameters of the FDM machines. Finally, all the FDM commands were exported in G-code files. A Sharebot Next Generation FDM printer was used for printing the samples. The speed of extruder head was set to 40 mm/s for printing moves and to 100 mm/s for travel moves and a rectilinear infill with 100% density was used. The temperature of the heated bed was set at 110 °C for every samples, while the extrusion temperatures were different for ABS samples (230 °C) and for nanofilled samples (255 °C). The samples were printed along three different orientations, named horizontal (HC), vertical (VC) and perpendicular (PC) configurations, respectively (see Fig. 1). For VC and PC samples detachable supports were printed to support the growing sample. In this way, it was possible to reach an optimal surface quality thank to the reduction of the oscillations of the samples during the printing processes. In Table 1 the list of the prepared samples is reported.

2.3. Experimental methodologies

2.3.1. Melt flow index (MFI)

MFI measurements were performed in order to evaluate the influence of the nanofiller introduction on the processability of the resulting materials. A Kayeness 4003DE capillary rheometer was used, and the tests were performed according to the ASTM D 1238 standard at a temperature of 220 °C and applied load of 10 kg.

2.3.2. Mechanical properties

An electromechanical Instron 4502 machine equipped with a 1 kN load cell was used for the tensile tests. For the determination of the elastic modulus (E), a cross-head speed of 1 mm/min was adopted, and the deformation values were measured through an electrical extensometer (Instron mod. 2620) with a gage length of 12.5 mm. Tensile properties at yield and at break were determined at a cross-head speed of 10 mm/min without extensometer. In both cases, ISO 527 1BA samples with a gage length of 30 mm were tested. Yield stress (σ_y) was taken in correspondence of the zero-slope tangent to the stress-strain curve while stress (σ_b) and strain (ε_b) at break were evaluated at the failure point.

Table 1
List of the samples tested in this work.

Notation	CNT content (wt.%)	Processing technique		
		Compression molding	Filament extrusion	3D printing
ABS	0.0	X	–	–
ABS-CNT-01	1.0	X	–	–
ABS-CNT-02	2.0	X	–	–
ABS-CNT-04	4.0	X	–	–
ABS-CNT-06	6.0	X	–	–
ABS-CNT-08	8.0	X	–	–
ABS-CNT-15	15.0	X	–	–
ABS-F	0.0	–	X	–
ABS-P-HC	0.0	–	X	X
ABS-P-VC	0.0	–	X	X
ABS-P-PC	0.0	–	X	X
ABS-CNT-06-F	6.0	–	X	–
ABS-CNT-06-P-HC	6.0	–	X	X
ABS-CNT-06-P-VC	6.0	–	X	X
ABS-CNT-06-P-PC	6.0	–	X	X

2.3.3. Electrical properties

Electrical resistivity measurements were carried out by using a Keithley 6517A electrometer following the ASTM D4496-04 standard for moderately conductive materials. A four points contact configuration was used and the tests were performed applying voltages of 2, 12, 24, 30 V at room temperature. The external electrodes of the apparatus were connected with an electrometer, in order to apply the voltage to the sample and to measure the current flow through the samples. The internal electrodes were connected at a fixed distance of 3.69 mm, in order to measure the voltage difference within the electrodes. In order to measure the resistivity, it was assumed that the samples were homogenous and behaved like ohmic conductors, neglecting possible capacitive or inductive effects. The electrical volume resistivity of the samples was therefore evaluated by Eq. (1):

$$\rho = R \cdot \frac{A}{L} \tag{1}$$

where R is the electrical resistance, A is the is the cross-section of the specimen and L is the distance between the internal electrodes (i.e. 3.69 mm).

The heating of a sample generated by a current flow is known as resistive heating and it is described by the Joule's law. Surface temperature evolution induced by Joule's effect upon different applied voltages was measured by a TiRx thermal imaging camera provided by Fluke. The voltages were applied by a DC power supply (IPS 303DD produced by ISO-TECH), while the samples were fixed with two metal clips with an external distance of 30 mm. In these tests, 50 × 6 mm samples with a thickness of 1.2 mm were used. The surface temperature values have been recorded after 0, 5, 10, 30, 60 and 120 s of application of voltage levels of 12 V and 24 V.

2.3.4. Thermal conductivity/diffusivity

Square plaques were produced with a side length of 12.7 mm and a thickness between 1.1 and 2.2 mm. Printed samples were produced in a horizontal build-up and were measured perpendicular to this direction.

For the determination of thermal properties laser flash measurements using a Netzsch LFA 447 were performed. The method consists in exposing one side of a disc sample with a thickness (d) [15] to an energy pulse from a light source (laser or xenon flash lamp) [20] and measuring the temperature history on the other side using a liquid nitrogen cooled infrared detector. Samples were measured at three different temperatures (25, 50 and 75 °C) performing 3 shots respectively. Data were analysed using the software Proteus. Thermal diffusivity (α) was calculated using Cowan method with pulse correction. For the determination of the heat capacity (c_p), a standard Pyrex 7740 reference material prepared according to ASTM-E 1461 was measured and compared with the samples. Additionally, sample density (ρ) was determined based on measured sample dimensions and mass, to calculate the thermal conductivity (λ) using the expression reported in Eq. (2):

$$\lambda = \alpha \rho c_p \tag{2}$$

3. Results and discussion

3.1. Melt flow index

The results of melt flow index tests are reported in Fig. 2. As expected, as the nanofiller amount increases the MFI decreases. A significant drop of MFI values can be observed for a CNT content of about 1 wt.%. It is therefore possible to conclude that the mechanical percolation of the CNTs is reached for nanofiller amounts higher than 1 wt.%, and the processability of the material is partially impaired for CNT contents higher than 4 wt%. It is worthwhile to report that ABS-CNT-15 sample resulted too viscous to be tested under the selected conditions (220 °C and 10 kg).

3.2. Mechanical behaviour

Representative stress-strain curves of ABS nanocomposite compression molded samples are reported in Fig. 3a, while the associated parameters are summarized in Table 2. As frequently observed for nanofilled samples [21], neat ABS presents a much higher strain at break compared with the filled samples, and nanofiller introduction induces a heavy embrittlement of the samples. If the neat masterbatch is considered (i.e. CNT loading of 15 wt%), the sample is very brittle, and the failure occurs before the yield point is reached. On the other hand, for intermediate amounts of nanofiller a progressive increase of the stiffness (E) and the stress at yield (σ_y) can be observed. On the basis of these considerations, ABS-CNT-04 and ABS-CNT-06 samples seem to represent an optimal compromise between the increase of the elastic modulus and the decrease of the elongation at break.

Representative stress-strain curves of 3D printed unfilled and CNT filled samples with a filler loading of 6 wt% are represented in Fig. 3b and c, respectively. The most important mechanical parameters are summarized in Table 3. Regardless the printing orientation, all FDM printed unfilled samples manifest a drastic loss of ductility and the fracture occurs at smaller strain values if compared with the neat ABS bulk specimens. The loss of ductility can be attributed to the reduction of cross section caused by the presence of voids in the specimens microstructure. For the same reason, also the elastic modulus is negatively affected by the FDM process. Furthermore, some considerations about the build configuration can be made: when tensile stress is perpendicular

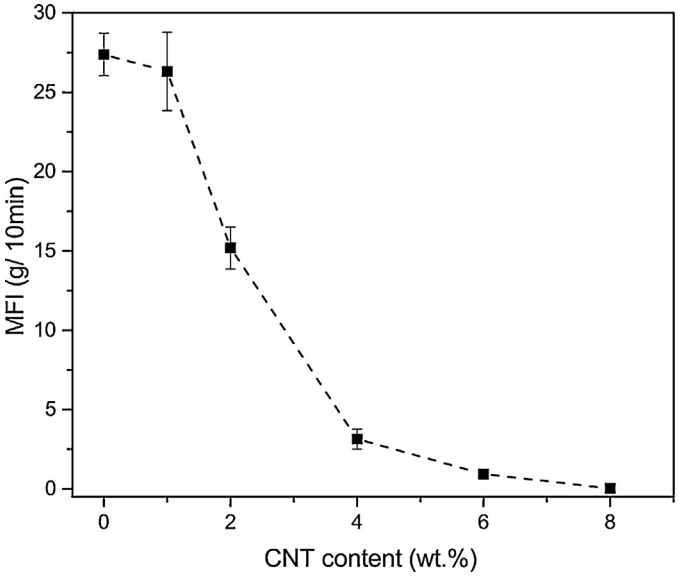

Fig. 2. MFI values of ABS nanocomposites as a function of CNT contents.

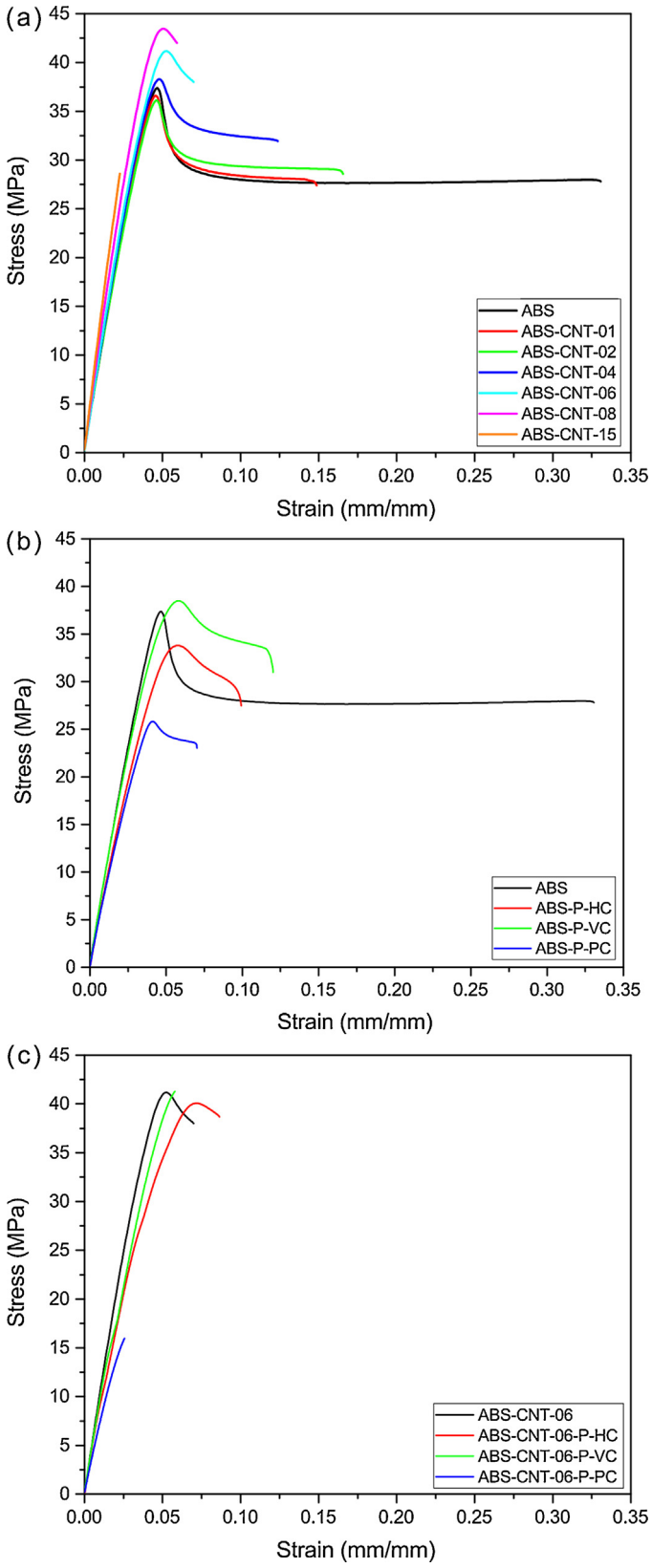

Fig. 3. Representative stress-strain curves of (a) ABS-CNT compression molded nanocomposites with different CNT contents, (b) 3D printed neat ABS samples along various orientations and (c) 3D printed ABS nanocomposites with 6 wt.% of CNT along different building orientations.

Table 2
Quasi-static tensile properties of compression molded ABS samples.

Sample	E [MPa]	σ_y [MPa]	σ_b [MPa]	ε_b [%]
ABS	2159.8 ± 63.5	37.3 ± 0.3	27.5 ± 0.7	35.4 ± 3.8
ABS-CNT-01	2169.1 ± 62.1	35.2 ± 1.1	26.9 ± 0.7	14.0 ± 2.8
ABS-CNT-02	2296.4 ± 96.7	36.0 ± 0.1	28.8 ± 0.3	11.5 ± 4.1
ABS-CNT-04	2552.6 ± 85.0	39.1 ± 1.1	32.7 ± 0.9	9.8 ± 1.7
ABS-CNT-06	2820.8 ± 122.1	41.7 ± 0.5	39.5 ± 1.3	6.8 ± 1.1
ABS-CNT-08	2856.2 ± 93.1	43.0 ± 1.2	42.3 ± 0.7	5.5 ± 0.5
ABS-CNT-15	2917.3 ± 177.5	–	22.0 ± 4.4	1.8 ± 0.4

Table 3
Quasi-static tensile properties of 3D printed samples.

Sample	E [MPa]	σ_y [MPa]	σ_b [MPa]	ε_b [%]
ABS-P-HC	2013 ± 152	34.0 ± 1.5	29.5 ± 1.6	9.3 ± 2.8
ABS-P-VC	2132 ± 139	38.8 ± 0.4	33.6 ± 3.6	8.3 ± 3.0
ABS-P-PC	1963 ± 70	25.1 ± 0.7	23.0 ± 0.1	6.4 ± 0.2
ABS-CNT-06	2821 ± 122	42.0 ± 0.5	39.5 ± 1.3	6.8 ± 1.1
ABS-CNT-06-P-HC	2487 ± 225	38.3 ± 3.3	36.8 ± 2.3	7.9 ± 1.3
ABS-CNT-06-P-VC	2633 ± 151	35.3 ± 2.0	37.9 ± 3.1	6.6 ± 1.7
ABS-CNT-06-P-PC	1987 ± 209	–	15.8 ± 4.6	2.3 ± 0.6

to the cross section of each layer (perpendicular configuration, PC), the fracture occurs between two layers and the samples exhibit low yield strength. However, if the sample is pulled along the cross section of the deposited roads (like in the vertical configuration, VC), the fracture occurs within the roads and the material exhibits a greater yield strength. Finally, when the tensile stress has a direction that is intermediate between the two previous cases (i.e. HC configuration), an intermediate behaviour can be observed for the ultimate mechanical properties.

It is worthwhile to observe that 3D printed specimens containing 6 wt% of CNTs (see Fig. 3c) manifest tensile modulus and strength values higher that the corresponding unfilled samples. Also in this case, the influence of the build configuration is clearly detectable, especially on the ultimate mechanical properties. The reduction of strain at break if compared with the compression molded samples is not so remarkable as in the case of neat ABS samples, because the bulk nanocomposites material is already embrittled by the presence of CNT. Anyway, in ABS-CNT-06-P-PC samples the fracture occurs for very small strain value, due to the combination of embrittling effect due to the nanofiller introduction and the unfavourable direction of the tensile stress with respect to layers orientation. However, it can be generally concluded that the reduction of the mechanical properties in 3D printed materials is not so heavy if compared with the corresponding compression molded samples (except for the ABS-CNT-06-P-PC sample), and this means that the FDM techniques can be potentially interesting as an alternative manufacturing method.

3.3. Electrical behaviour

3.3.1. Electrical resistivity

The measurement of electrical resistivity was crucial for the determination of the electrical percolation threshold and for establishing the CNTs content required to achieve an appreciable reduction of the electrical resistivity. The results of the electrical volume resistivity tests on the compression molded materials are reported in Fig. 4a. First of all, it is clear that the addition of CNTs is very effective in decreasing the electrical resistivity with respect to neat ABS even at small filler contents. Considering that the electrical resistivity of the neat ABS bulk sample is $10^{12}\,\Omega$ cm, the reduction of electrical volume resistivity is of about nine orders of magnitude for ABS-CNT-01 samples, while even better results can be obtained with the ABS-CNT-08 nanocomposites, for which a reduction of thirteen orders of magnitude is achieved. Moreover, the electrical resistivity of the loaded samples does not appreciably change with the applied voltage. It can be concluded that these materials behave like ohmic conductors. In Fig. 4b the electrical resistivity data of compression molded samples at an applied voltage of 12 V are plotted as function of CNT content. A significant resistivity drop can be achieved at CNT contents higher than 1 wt.%. This result is quite similar to that reported in literature for ABS/MWCNT nanocomposites [22] for which an electrical percolation threshold of 0.6 wt% is reported.

The electrical resistivity values of the extruded nanocomposites filaments (ABS-CNT-06-F) are very similar to those of the

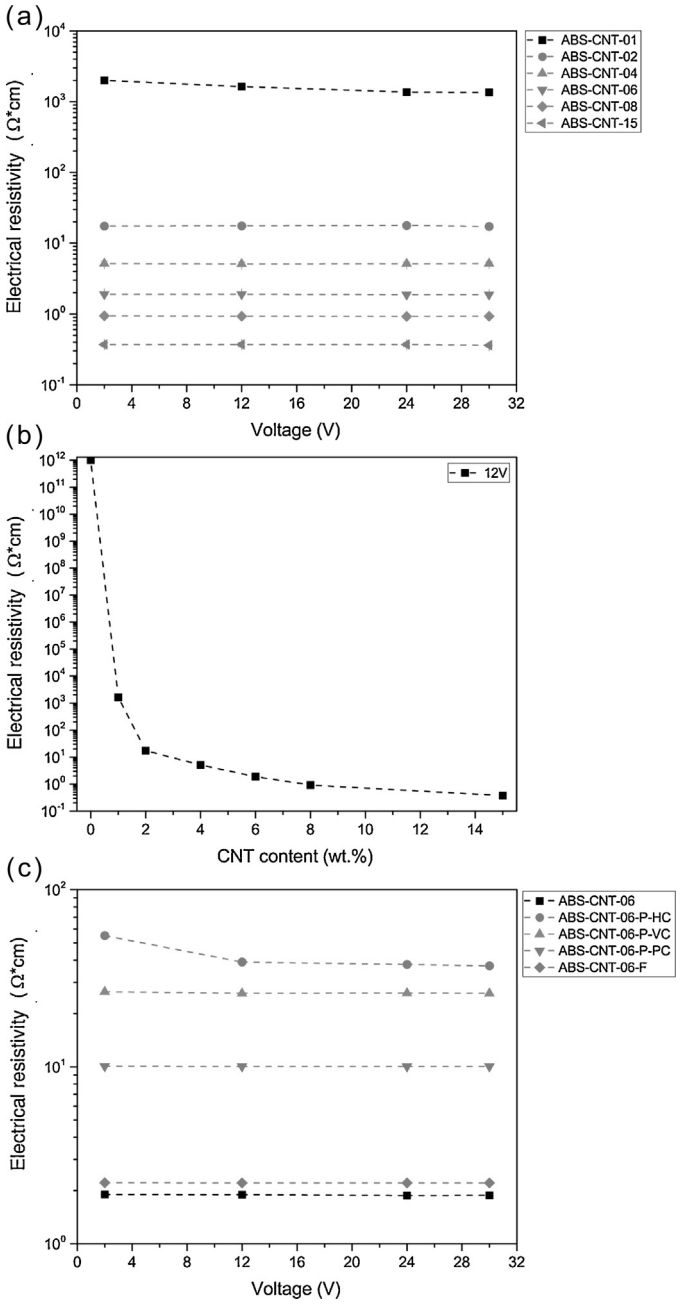

Fig. 4. Electrical resistivity of (a) ABS compression molded nanocomposites as a function of the applied voltage, (b) ABS compression molded nanocomposites at 12 V as function of CNT content and of (c) 6 wt.% filled nanocomposites with different building orientations.

compression molded samples materials and therefore are not reported for sake of brevity. The results of the electrical resistivity tests on the samples filled with 6 wt.% of CNT are reported in Fig. 4c. Comparing these data with those of compression molded plates, it can be observed that the 3D printing process determines a partial increase in the electrical resistivity, with a marked dependency on the 3D printing direction. The increase of electrical resistivity is greater for horizontal and vertical printing directions, while is less pronounced for the perpendicular one. The resistivity seems to be slightly dependent on the applied voltage, especially at low voltages, for the samples printed along the horizontal direction. This dependence cannot be detected in the other investigated directions where an ohmic behaviour was observed. This means that the experienced increase of electrical resistivity in 3D printed samples is probably due to the presence of contact resistances between the deposited filaments. However, further analysis are required for a better comprehension of this aspect.

3.3.2. Surface temperature under applied voltage

In this paragraph, the measurements of Joule's heating upon voltage application of the samples with different contents of CNT are presented. These tests were performed by using two different voltages, 12 V and 24 V. These two values were chosen because they are the most common voltages for lead–acid batteries used in cars and trucks. Representative images of the evolution of the surface temperature taken by an IR thermocamera under an applied voltage of 24 V for the ABS-CNT-06 nanocomposite is reported in Fig. 5. It is immediately evident that the samples can be rapidly heated if a voltage is applied, and a homogeneous temperature profile can be detected even after prolonged time (i.e. 120 s). As it could be expected, the temperature in the central section of the sample is higher than that detectable on the borders, because the heat exchange is favoured in the external zones of the samples.

The numerical results of the temperature increment upon an applied voltage of 12 V and 24 V are shown in Fig. 6a and in Fig. 6b, respectively. The first aspect to underline is that not all the samples can be significantly heated through the voltage application. In fact, only samples with CNT content higher than 4 wt.% can increase their surface temperature when a voltage of 12 V is applied. On the other hand, it was not possible to complete the test of ABS-CNT-15 because after 30 s it started to decompose by thermal degradation.

At an applied voltage of 24 V, only ABS-CNT-01 sample does not significantly increase its surface temperature, while ABS-CNT-02 shows a moderate heating after 120 s. Very effective results can be obtained for all the other samples: none of them was able to reach the end of the test because they thermally decompose with emission of a dense smoke, characteristic of polymers containing aromatic rings [23]. Another interesting aspect common to both groups of measurements (under 12 V and 24 V) is that the samples are not able to reach a temperature plateau within the experimental time interval, corresponding to a condition in which the generated power is equal to the dissipated one.

The measurements of Joule's heating effect upon voltage application of 3D-printed samples were performed by using the same two voltages applied to the CM materials (12 V and 24 V) on samples with CNT contents of 6 wt.% built along different orientations. The results of the measurements at 12 V are reported in Fig. 7a. The loss in electrical conductivity experienced on 3D printed materials determines a reduction of the surface temperature increment in the samples with horizontal and vertical configurations. The temperature evolution trends of the 3D printed materials in the perpendicular configuration are very similar to those reported for the corresponding CM materials. This result can be explained considering the better retention of electrical conductivity for the 3D printed materials under this configuration.

The results of the measurements at 24 V are shown in Fig. 7b. All the printed samples tested at this voltage show a behaviour that differs from that observed on CM materials. First of all, the temperatures reached are much lower than the ones registered on the CM materials. Moreover, the samples seem to reach a plateau of almost constant temperature after 60 s of testing. However, a significant heating can be obtained also for printed materials, and the presence of a thermal plateau for prolonged voltage application

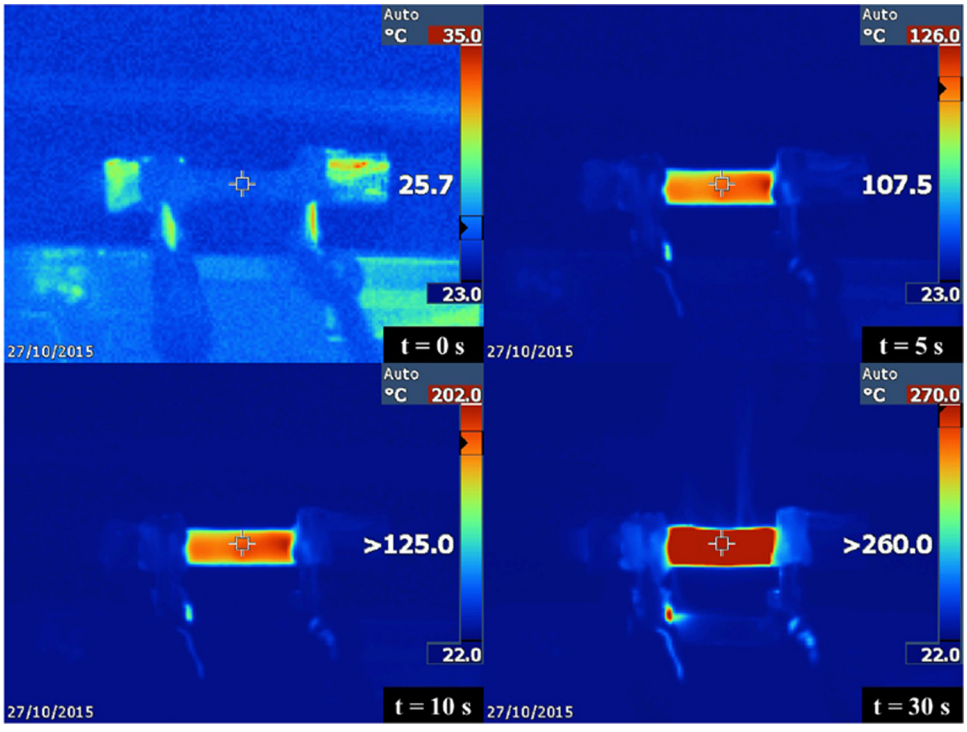

Fig. 5. Infrared thermal imaging of ABS-CNT-06 nanocomposite samples under an applied voltage of 24 V.

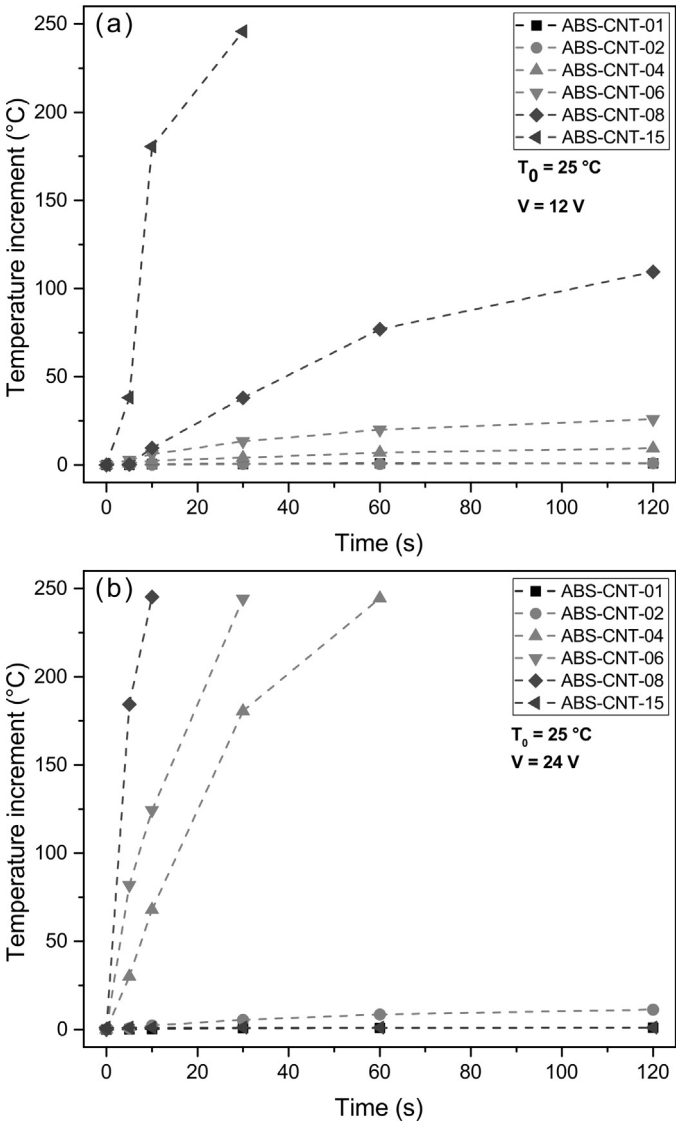

Fig. 6. Increment of surface temperature upon an applied voltage of (a) 12 V and of (b) 24 V for ABS-CNT compression molded nanocomposites with different CNT contents.

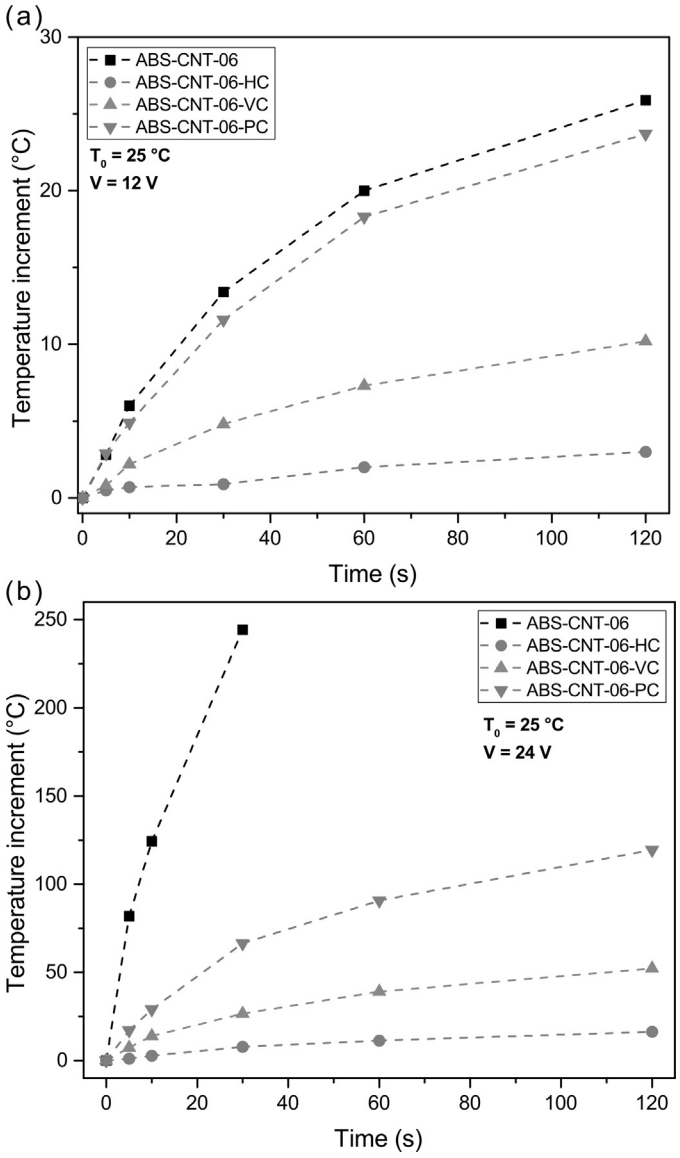

Fig. 7. Increment of surface temperature for 6% wt. of CNT nanocomposite samples 3D printed along different orientations under an applied voltage of (a) 12 V and of (b) 24 V.

time can be important for technological applications in which the thermal degradation of the device should be hopefully avoided.

3.4. Thermal conductivity/diffusivity

Thermal properties parameters measured on the investigated samples are presented in Fig. 8(a–c). The specific heat (Fig. 8a) of ABS and ABS-CNT-06 compression molded samples differs by about 11% at 25 °C. No significant difference between CM and 3D printed samples can be observed. In Fig. 8b the thermal diffusivity values are reported. The lowest values were found for ABS. An addition of 6 wt.% CNT results in an increase of about 55% of thermal diffusivity (ABS-CNT-06-P-HC at 25 °C). Comparing CM and 3D printed samples an opposite trend can be observed for neat ABS and nanocomposite samples. In fact, the value of ABS-P is about 24% higher than for ABS while a decrease of thermal diffusivity about 7% was observed between ABS-CNT-06 and ABS-CNT-06-P-HC.

Considering the reported results of thermal conductivity of ABS and ABS-CNT-06 samples (Fig. 8c), an increase of about 42% was achieved by adding CNT to neat ABS [24,25]. Interestingly the production process has a strong impact on thermal conductivity of the samples containing CNT. While ABS and ABS-P samples show similar thermal conductivity values, a significant decrease (about 21%) was observed for ABS-CNT-06 and ABS-CNT-06-P-HV samples. This could be tentatively attributed to a unfavourable orientations achieved by CNT after the FDM process [26].

4. Conclusions

Multi-walled carbon nanotubes were dispersed in an ABS matrix through a masterbatch at different concentrations, and the resulting materials were extruded in filaments suitable for the fused deposition modelling process. Samples were then 3D printed by using different printing orientations. The most important properties of the compression molded and 3D-printed materials were studied.

The stiffness and the yield properties of the bulk samples were increased by nanofiller addition, while strain at break values were negatively affected by CNT introduction. 3D printed unfilled samples presented a drastic loss of ductility if compared with the

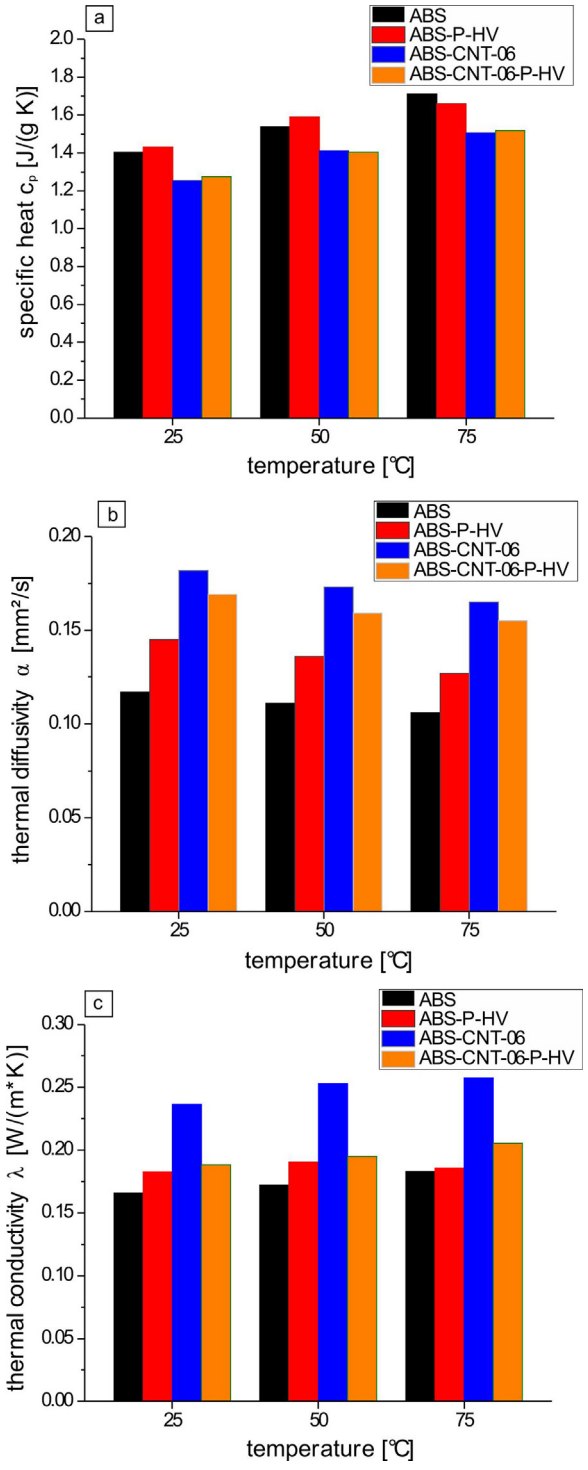

Fig. 8. Thermal properties of compression molded and 3D printed nanocomposites. (a) Specific heat, (b) thermal diffusivity and (c) thermal conductivity values.

neat ABS CM specimens, with a strong dependency on the 3D printing direction.

The electrical resistivity was strongly decreased by CNT addition even at limited (i.e. 1 wt%) filler contents, while the 3D printing process led to a partial loss in the electrical conductivity, especially in horizontal and vertical configurations. As a consequence, the loss in electrical conductivity due to the printing operation led to a reduction of the surface temperature increment in the printed samples.

Thermal properties of neat ABS were significantly influenced by the addition of CNT. While a decrease of specific heat c_p (−11%) was observed, thermal diffusivity α (+55%) and conductivity λ (+30%) increased with a CNT amount of 6 wt% for bulk materials at 25 °C. The production process influenced thermal diffusivity and conductivity, specific heat seemed to be equal for ABS and ABS-CNT-06. While thermal diffusivity increased for ABS/ABS-P sample (+24%), a decrease for ABS-CNT-06/ABS-CNT-06-P-HV (−7%) was observed. Interestingly, printing process led to no significant change in thermal conductivity for ABS/ABS-P, but had high impact on ABS-CNT-06/ABS-CNT-06-P-HV (−21%), which may be the result of an partial CNT orientation.

References

[1] M. Rong, M. Zhang, Y. Zheng, Polymer 42 (2001) 3301–3304.
[2] X. Fu, S. Qutubuddin, Mater. Lett. 42 (2000) 12–15.
[3] J.S. Shelley, P.T. Mather, K.L. De Vries, Polymer 42 (2001) 5849–5858.
[4] Z. Shu, G. Chen, Z. Qi, Plast. Ind. 28 (2000) 24–26.
[5] F.M. Uhl, C.A. Wilkie, Polym. Degrad. Stab. 76 (2002) 111–122.
[6] T. Agag, T. Koga, T. Takeichi, Polymer 42 (2001) 3399–3408.
[7] R.H. Norman, B.B. Boonstra, J. Polym. Sci. Part B: Polym. Lett. 10 (1972) 479.
[8] M. Armad, Adv. Mater. 2 (1990) 278–286.
[9] T.A. Ibidapo, Polym. Eng. Sci. 28 (1988) 1473–1476.
[10] A. Maiti, A. Svizhenko, M.P. Anantram, Phys. Rev. Lett. 88 (2002) 126805.
[11] R. Ou, R.A. Gerhardt, C. Marrett, A. Moulart, J.S. Colton, Compos. Part B-Eng. 34 (2003) 607–614.
[12] M.L. Terranova, S. Orlanducci, E. Fazi, V. Sessa, S. Piccirillo, M. Rossi, D. Manno, A. Serra, Chem. Phys. Lett. 381 (2003) 86–93.
[13] B. Berman, Bus. Horiz. 55 (2012) 155–162.
[14] I.J. Petrick, T.W. Simpson, Res. Technol. Manage. 56 (2013) 12–16.
[15] M.H. Al-Saleh, H.K. Al-Anid, Y.A. Hussain, Compos. Part A: Appl. Sci. Manuf. 46 (2013) 53–59.
[16] X. Wei, D. Li, W. Jiang, Z. Gu, X. Wang, Z. Zhang, Z. Sun, Sci. Rep. 5 (2015) 11181.
[17] S. Dul, L. Fambri, A. Pegoretti, Compos. Part A: Appl. Sci. Manuf. 85 (2016) 181–191.
[18] M.L. Shofner, F.J. Rodriguez-Macias, R. Vaidyanathan, E.V. Barrera, Compos. Part A-Appl. Sci. Manuf. 34 (2003) 1207–1217.
[19] J.M. Gardner, G. Sauti, J.-W. Kim, R.J. Cano, R.A. Wincheski, C.J. Stelter, B.W. Grimsley, D.C. Working, E.J. Siochi, Addit. Manuf. 12 (2016) 38–44.
[20] W.J. Parker, R.J. Jenkins, C.P. Butler, G.L. Abbott, J. Appl. Phys. 32 (1961) 1679.
[21] D. Pedrazzoli, A. Dorigato, T. Conti, L. Vanzetti, M. Bersani, A. Pegoretti, Express Polym. Lett. 9 (2015) 709–720.
[22] B.K. Singh, P. Kar, N.K. Shrivastana, B.B. Khatua, J. Appl. Polym. Sci. 124 (2012) 3165–3174.
[23] J.V. Rutkowski, B.C. Levint, Fire Mater. 10 (1986) 93–105.
[24] M.K. Samani, N. Khosravian, G.C.K. Chen, M. Shakerzadeh, D. Baillargeat, B.K. Tay, Int. J. Therm. Sci. 62 (2012) 40–43.
[25] D.J. Yang, Q. Zhang, G. Chen, S.F. Yoon, J. Ahn, S.G. Wang, Q. Zhou, Q. Wang, J.Q. Li, Phys. Rev. B 66 (2002).
[26] J. Hone, M.C. Llaguno, M.J. Biercuk, A.T. Johnson, B. Batlogg, Z. Benes, J.E. Fischer, Appl. Phys. A: Mater. Sci. Process. 74 (2002) 339–343.